Experimental investigation of the exit dynamics of a horizontal circular cylinder out of water and silicone oil

Intesaaf Ashraf [1], Lionel Vincent [2,3], Romain Falla [4], Vincent E. Terrapon [4], Benoit Scheid [2], and Stéphane Dorbolo [1]

[1]*PtYX, Département de Physique, Université de Liège, 4000 Liège, Belgium*

[2]*Department of Transfers, Interfaces, and Processes, Université Libre de Bruxelles, 1050 Brussels, Belgium*

[3]*Campus Innovation Paris, Air Liquide Research & Development, 1, chemin de la Porte des Loges, Les Loges-en-Josas, France*

[4]*Department of Aerospace and Mechanical Engineering, Université de Liège, 4000 Liège, Belgium*

Experimental investigations of the exit dynamics of a horizontal cylindrical object were performed in water and silicone oil (50 cS). The fully immersed cylinder was initially at rest in a still fluid tank before being pushed (or pulled according to the measurement procedure) upwards at a constant velocity. The cylinder geometry was chosen to approach two-dimensional conditions in the transverse direction. First, we demonstrate that these conditions are better satisfied for a large aspect ratio cylinder equipped with vertical end plates. Second, the influence of the initial depth on the liquid entrained and the wake generated by the cylinder is discussed. It is shown that the wake destabilizes in the form of symmetry breaking in the case of water, while it remains symmetrical in the case of oil even for long travel in the bath. The deformation of the interface is found to be independent of the starting depth when the starting depth is larger than six times the cylinder diameter. In the present case, this criterion reflects also the finite acceleration of the cylinder to reach the determined constant exit velocity. Measurements in a range of exit speeds between 0.1 and 1 m/s indicate that the thickness of the liquid above the cylinder when the cylinder starts crossing the interface increases with the speed according to a logarithmic law of the Froude number. During the subsequent drainage, the evolution of the coated liquid thickness is found to first decrease exponentially with time just after the crossing of the interface. At later times, a change of regime occurs and the drainage follows the inverse of the square root of time irrespective of the crossing speed. Finally, the force necessary to maintain a constant exit speed during the motion of the cylinder inside and outside the bath is analyzed. This global measurement of the entrained liquid confirms the square root scaling of the thinning with time during the drainage process.

I. INTRODUCTION

The physics of a body entering or exiting a liquid bath has been the subject of numerous studies, mostly driven in recent years by space (e.g., the splashdown of spacecraft), military (e.g., missile launching by submarines), and industrial (e.g., coating) applications. Water entry and exit problems are also commonly found in nature, for instance, animals jumping out of the water [1] or animals diving in the water [2]. In both cases, accurate experimental measurements, theoretical analysis, and numerical simulations are challenging because of the complexity of the phenomena to take into account, such as interfacial physics and fluid-structure interactions.

While research on water entry has primarily focused on optimum design, shape, and entry velocity [3–8], the water entrainment after the exit is of particular interest. Indeed, the exit problem

is closely related to the drainage process of the entrained liquid. Depending on the applications, fast drainage might be required (missiles, fishing birds), or, on the other hand, slow and uniform drainage might be more beneficial. For instance, when an object has to be coated with paint, the simplest way to proceed is to plunge the object into a large bath and pull it out of the bath. The speed of pulling, the viscosity, and the surface tension of the fluid, as well as the contact angle, have to be taken into account for the coating of the surface parallel to the pulling direction.

This problem of the extraction of a solid from a liquid was addressed in the work by Landau, Levich, and Derjaguin (LLD) in the case of a vertical plate that is extracted from viscous liquids and/or with small velocities [9,10]. The configuration is rather generic and is found in numerous industrial processes involving the dip coating of a surface to transform its property (coloring, anti-scratching, antiwetting, antioxidizing, etc.). Studies have shown the richness of the LLD problem by considering the effects on the liquid entrainment of complex fluids [11], solid microtextures [12], and solid elasticity [13]. These researches have improved the reliability and the control of the dip-coating process. Some works have also considered the influence of the inclination, either of the substrate [14], of the pulling direction [15], or even along the bottom face of the object [16,17]. The subsequent liquid film drainage along flat or curved surfaces is another field that has extensively been studied since Reynolds's seminal work [18] and is still very active [19,20]. However, the LLD problem refers to objects that are partially immersed in their initial position. The total amount of liquid entrained by lifting an object as simple as a sphere out of a bath remains an open question [21].

The manner to extract the object from the bath is a key to determining the drainage dynamics. Concerning the water exit problem, the extraction can be categorized according to different parameters. The body motion can be forced through an imposed displacement [22,23] or an external force [24], driven by buoyancy [25] (e.g., when playing with a balloon in a swimming pool [26]) or a combination of an initial forced motion followed by an inertial phase [27]. Regarding the shape of the body, most works have focused on rather canonical shapes, including spheres [22,25,27,28], vertical cylinders [23,29], horizontal cylinders [30–33], prolate ellipses [34], or even square cylinders [35].

In the present paper, we focus on the extraction of a horizontal cylinder out of a bath of liquid with a constant velocity. The motivation for studying the horizontal cylinder exit is to restrict the flow around the object to mimic and approximate two-dimensional (2D) conditions for the flow around the section of the object. We chose to study constant speed conditions since they are encountered in numerous situations and since the speed during the crossing of the interface can be approximated to be constant carriage return. The water exit of a horizontal cylinder has already been addressed in some previous works.

Greenhow and Lin [31] performed inspiring experimental works. A few years later, the same group [32] published two-dimensional numerical simulations of the free-surface deformation of an initially calm water surface. In this paper, the experimental data set can be found for a "short" cylinder (the length being two or three times the diameter of the cylinder).

A more extensive work was proposed by Haohao *et al.* [36], including the case of the sphere. Both numerical simulations and some experimental results were presented. A cylinder with an aspect ratio (length divided by radius) of 4 was equipped with vertical end plates to keep the velocity field parallel to the direction of motion. The measurements were compared to a model CIP (constrained interpolation profile) based on a work by Miao [37] with good agreement for a reduced set of imposed conditions. Additionally, simulations were carried out at four different Froude numbers (defined as the square of the object's speed divided by the gravity times the radius of the object). The free-surface elevation when the cylinder starts crossing the interface was found to be strongly dependent on the Froude number for values below 4.12. However, for large speeds (Froude number between 4.12 and 8.24), the time dependence of the surface elevation was nearly the same. Finally, these authors reported that waterfall breaking becomes more intense as the Froude number increases due to the vortex generated in the wake. On the other hand, the waterfall reduces to a ligament at low speeds. Note that, beyond the waterfall, the liquid that flows around the cylinder may also destabilize into a ligament. In this case, the coating thickness was reported numerically in a recent paper [38].

Moshari *et al.* [24] numerically investigated the problem of the exit of the horizontal cylinder using a method based on volume of fluids from the starting depth until the dewetting of the cylinder. The motion was driven by applying a constant force and the considered starting depths were less than three times the cylinder diameter. Both 2D and three-dimensional (3D) simulations were performed, which allowed determining the motion of the free interface (2D case) and showing some interesting dewetting phenomena (3D case) along the cylinder after the cylinder crossed the liquid interface. This dewetting could be observed in the case of a hydrophobic coated cylinder for example.

From a physical point of view, the drainage depends on the amount of liquid entrained, and thus on the characteristics of the interface crossing, but also on the flow dynamics during the initial immersed phase (e.g., wake behind the object). The challenge is that the liquid thickness above the object varies by more than four orders of magnitude during the entire process, i.e., the cylinder is first below the surface ($\approx$ m) and the lubrication drainage starts when the thickness of the film is below $100\,\mu$m.

II. FRAMEWORK

The present paper aims to provide experimental data on the complete motion of a horizontal cylinder crossing the interface, including (i) the elevation of the fluid surface during the motion of the cylinder inside the bath, (ii) the crossing over, (iii) the entrainment of the fluid, and eventually (iv) the link with the drainage of the fluid around the cylinder. The experimental setup and the choice of the cylinder aspect ratio were designed such as to approach a two-dimensional flow around the cylinder, namely invariant data regarding any translation along the axis of symmetry of the cylinder.

Two strategies were envisaged to reach 2D conditions of the flow around the cylinder. The aspect ratio AR defined as the ratio between the length L and the radius a of the cylinder can be increased in such a manner that the flow close to the ends of the cylinder influences less and less the experimental results. The second strategy consists of adding vertical end plates to the cylinder to force the fluid to flow perpendicularly to its symmetry axis. Based on particle imaging velocimetry (PIV) measurements, we will show that a large AR and the vertical end plates are required to obtain conditions as close as possible to 2D.

The starting depth d is an important parameter regarding the development of the cylinder wake. PIV was performed to characterize the fluid motion before the crossing. In the present experimental setup, the results are independent of the starting depth when $d > 12a$ considering the acceleration distance required to reach a constant velocity.

The measurements were performed for two fluids: water and silicone oil (50 cS). The aim of studying such different liquids was twofold: to assess the influence of the fluid kinematic viscosity ν, quantified by the Reynolds number $\mathrm{Re} = \frac{2Ua}{\nu}$, but also to address the dewetting around the cylinder. In particular, fast dewetting was observed with water because the cylinder was made out of metal. This could be mitigated with the oil, such that a slow drainage of the entrained fluid around the cylinder could be achieved over a larger range of time.

In practice, for a given fluid, using the most appropriate cylinder (largest AR with or without end plates) and starting with a sufficiently large depth, only one parameter is to be tuned: the imposed vertical speed U of the cylinder, adimensionalized by the Froude number, $\mathrm{Fr} = U^2/ga$, where g is the acceleration due to gravity. The time evolution of the height of the fluid interface above the cylinder, the local film thickness, and the force necessary to keep the speed constant were measured for different speed values.

The experimental setup is described in Sec. III, including the different measured quantities. A typical experiment is also presented to provide a qualitative description of the different regimes (see also some examples in the Supplemental Material [39]). The experimental conditions and limitations can be found in Sec. IV, with a detailed discussion about (i) the size of the cylinder and how to reach the 2D conditions, and (ii) the influence of the starting depth on the experimental results. It is important to mention that, as already stated, we will show that end plates and high aspect ratio cylinders are both required to reach 2D conditions. Consequently, most of the experimental

results presented in this paper were obtained for the AR = 12 cylinder equipped with end plates. Nonetheless, two experiments were performed under different conditions, namely the film thickness direct measurements (AR = 10 was used) and the force measurements (AR = 12 was used but without end plates). The reasons for these choices are given in the corresponding sections.

The measurements of the interface deformation during crossing are summarized in Sec. V. The upper position of the interface was recorded as a function of the position of the cylinder between an arbitrary starting time (defined when the top of the cylinder reaches the position of the interface at rest) and the crossing time (defined when the bottom of the cylinder reaches the position of the interface at rest). By image analysis, the maximum height reached by the air-fluid interface was detected as a function of the position of the cylinder during the motion. Knowing the position of both the interface and cylinder, the thickness h of the fluid above the cylinder can be quantified and analyzed. The vertical speed of the cylinder was tuned between 0.1 and 1.0 m/s (Sec. V A). The final stage of the drainage was studied using a chromatic confocal point sensor (CCPS, see Sec. V B), which allowed a direct measurement of h as a function of time. However, the CCPS was used only in the case of silicone oil because the water dewetted too quickly on the aluminum cylinders, preventing any meaningful measurements before dewetting.

During the uniform vertical motion of the cylinder, the force necessary to maintain a constant speed changes because of the time variations of three elementary contributions: drag, buoyancy, and liquid entrainment. The force was measured (Sec. VI) as a function of the position of the cylinder (or, equivalently, as a function of time) for different speeds U. The cases of water and oil are compared for the largest cylinder aspect ratio considered in this paper, AR = 12, to approach as best as possible 2D conditions. However, end plates were not used due to their large influence (friction drag and entrainment of extra liquid) on the force measurements. Finally, global conclusions are drawn in Sec. VII.

III. EXPERIMENTAL SETUP

The experimental setup consisted of a large fluid tank fitted with a lifting system that was used to pull or push the cylinder through the air-liquid interface. For the measurements, we used one or two synchronized high-speed cameras, a force sensor, a film thickness measurement device (CCPS), and a PIV system.

Figure 1 (top) presents three different measurement configurations of the experimental setup that are developed here below, namely the pushing mode (left), the film measurement (center), and the pulling mode (right).

The fluid tank was made of glass in the case of water and of PVC in the case of silicone oil with dimensions of $78.5 \times 72.5 \times 27.5$ cm for the length, height, and width, respectively. The lifting system was composed of a stage that moved along a linear guide. The motion was induced by a toothed belt entrained by a step motor. The cylinder under test for experiments was screwed to the stage via the carbon tube. The axis of symmetry of the cylinder was always oriented parallel to the fluid surface and was fixed on the moving frame by a rod that was screwed at one point of the symmetry plane of the cylinder. The frame pushed the cylinder upwards so that the fluid surface could only be deformed by the top side of the cylinder. However, in the case of the force measurements, the cylinder was connected to the stage only using one carbon fiber tube and was pulled upwards instead of pushed. This allowed us to reduce the influence of the frame (weight and liquid entrainment). To reach the constant speed set by the user, the acceleration was set to the maximum allowed by the motor, i.e., 4 m/s^2. In so doing, the cylinder could cross the interface with a constant speed between 0.1 and 1.3 m/s. The experiments were carried out at a room temperature equal to $20 \pm 2°$C.

The cylinder was made out of aluminum and had a smooth surface. Two types of cylinders were manufactured. One cylinder family had a radius $a = 25$ mm for lengths between 25 and 250 mm corresponding to aspect ratios AR = 1, 2, 4, 6, 10. Another cylinder type had a smaller radius
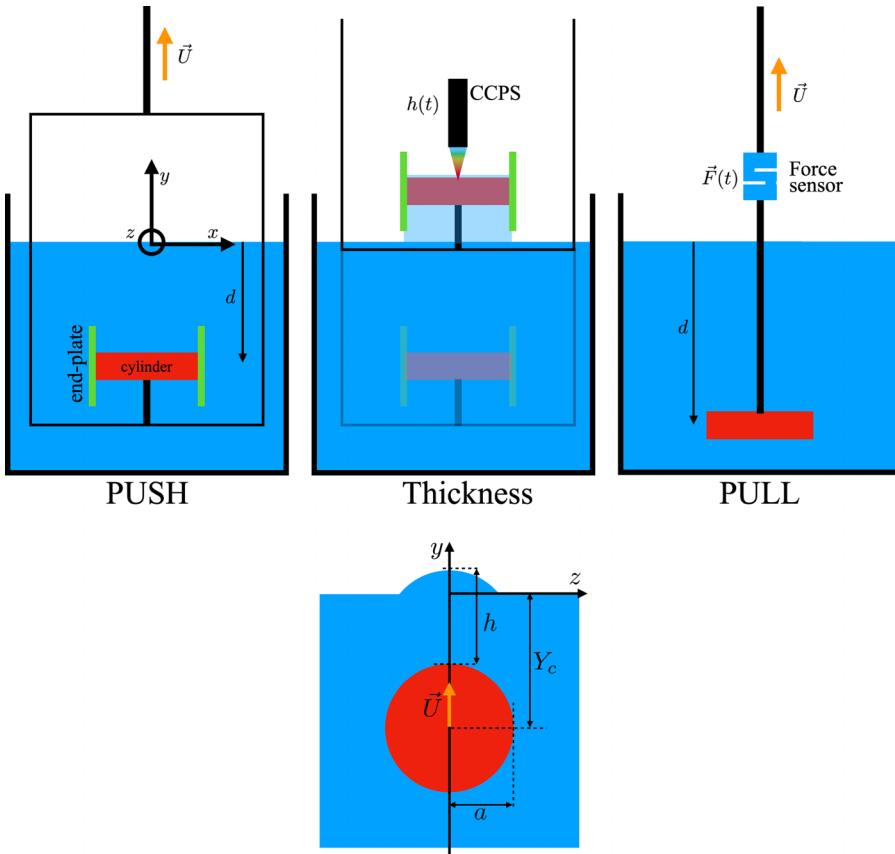
FIG. 1. Top: Schematic representations of the experimental configurations considered in this paper. Push mode: The cylinder was attached by the bottom and pushed upwards via a light rigid frame. End plates were added for some experiments to improve 2D conditions. Pull mode: The cylinder was attached by the top in order to limit the impact of the frame in the force measurements. Central panel: The cylinder can be stopped at a defined position to measure the oil film thickness evolution with time using a chromatic confocal point sensor (CCPS). Bottom: Sketch of the different parameters used in the paper.

$a = 12.5$ mm to achieve the largest considered aspect ratio, AR = 12. The end plates were added to the cylinder for some experiments (as specified in the text). The end plates were 200 mm in diameter and 4 mm in thickness for the cylinders with the larger radius, and 150 mm in diameter for AR = 12 with the same thickness.

The coordinate system (xyz) is shown in Fig. 1. The x axis is oriented along the length of the tank, and the z axis is along its width. The origin was set at the "at rest" free fluid-air interface considered as the horizontal plane of reference (xz). The pushing or pulling y axis passes by the origin and is aligned with the vertical direction. The coordinate Y_c designates the vertical position of the center of mass of the cylinder. The coordinate $y_c = Y_c/a$ is then normalized by the radius of the cylinder, a. The position $y_c = 0$ is defined as the position of the cylinder for which the cylinder is half plunged in the bath. Consequently, $y_c = -1$ corresponds to the position when the top of the cylinder touches the fluid surface from the bottom; the cylinder is completely above the surface when $y_c > 1$.

Two of the dimensionless parameters in this paper are the Froude and Reynolds numbers, which are varied by changing the cylinder exit velocity and the fluid viscosity. As mentioned earlier, two different kinds of fluids were used, i.e., water and silicone oil (50 cS, PMX-200). The specific density of oil is 0.96 and the kinematic viscosity is 5.0×10^{-5} m^2/s at 20 °C.

A. Measurements

Different experimental techniques were used for the different stages of the cylinder crossing.

1. Particle velocimetry measurements. A 2D planar PIV system was used for investigating the flow during the initial phase when the cylinder was still fully immersed. For the PIV exploration, the Light Amplification by Stimulated Emission of Radiation (LASER) had a wavelength of 532 nm and a peak power of 4 W. The seeding particles were about 20 μm in size. The postprocessing of the PIV images was done with the open-source software PIVLAB [40].

2. Fluid surface deformation. A white backlight (Effilux LED) was used to illuminate the cylinder and the fluid surface. Two high-speed M-310 phantom cameras acquired images at a rate of up to 3200 Hz. The cameras were perpendicular to the tank so that their respective field of view allowed a complete visualization of the crossing. The air-fluid interface was set in the middle of the image to reduce the parallax and to allow the tracking of the interface position.

3. Force measurements. A strain gauge SCAIME K25 (20 N) measured the force acting on the cylinder during the whole motion (from the initial acceleration to the end of the drainage). The gauge was calibrated using known weights. The data acquisition was performed using a datalogger (Picolog). The camera trigger signal was also recorded by the Picolog, which allowed the synchronization of the force measurements and the images captured by the camera. The force on the pulling rod was also measured in the absence of any cylinder to subtract the contribution of the rod and the corresponding entrained liquid from the measured force.

4. Thinning of the film. The drainage of the silicone oil located at the top of the cylinder was slow compared to that of the water. Specifically, in this latter case, the film broke up and dewetting was nearly instantaneous after the passage of the cylinder through the interface. On the other hand, the oil wetted well the cylinder. Once the cylinder had exited the bath, a CCPS (STIL, OPTIMA+) was used to record the thickness of the oil film located at the summit of the cylinder as a function of time. The measurement was achieved when the cylinder was at rest. Consequently, the cylinder had to be stopped in the measurement range of the CCPS. Moreover, the deceleration occurred when the cylinder was far above the interface in order to ensure a constant speed during the whole crossing process. For the largest considered speed, the cylinder needed a distance of approximately 17 cm to accelerate from rest to the aimed speed and the same distance to decelerate to rest. The cylinder was thus stopped about 30 cm above the surface of the bath to allow the complete crossing of the cylinder before deceleration.

B. Description of a typical experiment

A typical experiment began by positioning the cylinder at a desired initial position d in the tank. The initial position may vary for each set of experiments according to what was measured and to the presence or not of end plates. Ideally, d should be as deep as possible to ensure that the target speed was reached as deep below the surface as possible. Once the cylinder settled, a latency time of 15 min was observed so that all the surface waves were damped.

At this point, the cylinder was moved upward from its initial position at a constant acceleration γ of 4 m/s^2 until reaching the desired speed U. Then, the upward movement continued at a constant speed. For example, it took a distance of about 120 mm for the cylinder to reach a speed of 1.0 m/s. When the cylinder moved upward at a constant speed, the system went through different stages, as illustrated in Fig. 2 for a cylinder of aspect ratio AR = 12 and velocity U = 1.0 m/s (i.e., a Froude number Fr = 8.2) in water.

Stage 1 starts when the cylinder is far below the surface and initially moves without visibly disturbing the free surface. At a certain depth, the free surface starts deforming: it elevates and
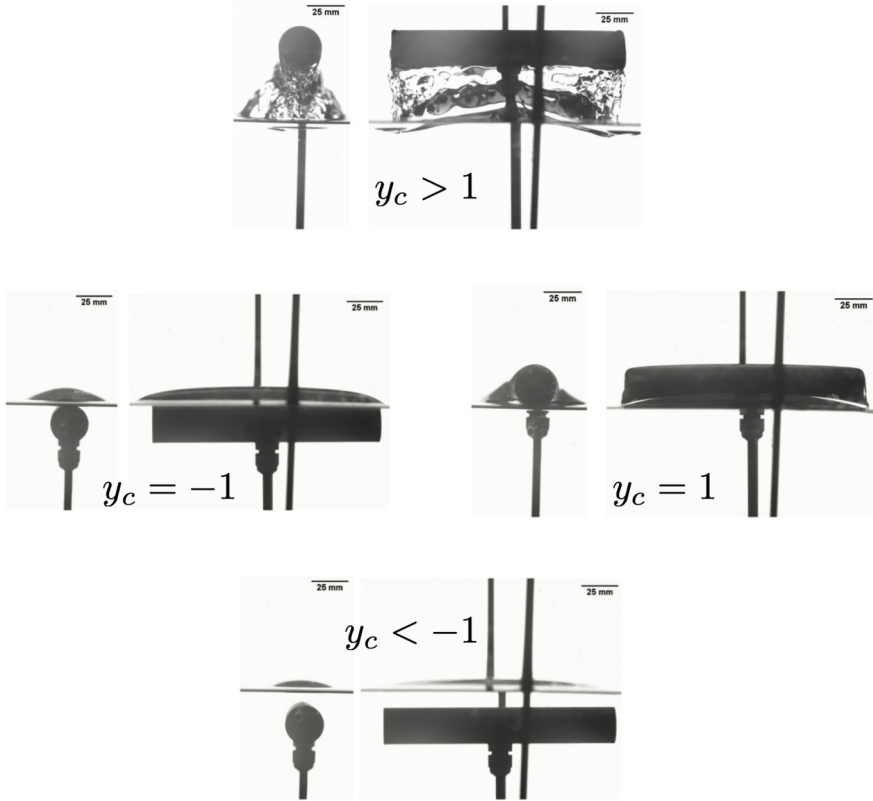
FIG. 2. Front and side views of the cylinder moving in the water and exiting the water surface for $AR = 12$ at $Fr = 8.2$. The origin of time $t = 0$ s is when $y_c = 0$. The different stages are (i) the motion in the fluid ($y_c < -1$), (ii) the beginning of the crossing when $y_c = -1$ to the end of the crossing when $y_c = 1$, and (iii) the liquid falling ($y_c > 1$).

presents a visible bumplike profile (see Fig. 2) until the cylinder starts crossing the interface. The thickness $h[y_c(t)]$ refers to the vertical distance between the top of the cylinder and the surface elevation at time t [see Fig. 1 (bottom)], and $h^* = h(y_c = -1)$ corresponds to the thickness at the specific moment when the top of the cylinder reaches the surface of the bath at rest. The thickness $h[y_c(t)]$ was tracked using high-speed cameras and the flow inside the bath was measured using PIV.

Stage 2 is the crossing over, also called the bulging regime. The crossing starts when the top of the cylinder reaches the initial position of the free water-air interface, i.e., at $y_c = -1$ (see Fig. 2). The time $t = 0$ s is set at the moment when the cylinder axis of symmetry crosses the interface ($y_c = 0$), such that $y_c = Ut/a$ during the constant velocity phase. The crossing ends when the bottom of the cylinder reaches the initial position of the interface, i.e., at $y_c = 1$, and from that moment, the interface profile starts resembling that of the cylinder.

Finally, stage 3 corresponds to the waterfall breaking and then ligament fragmentation [38].

The drainage stage starts immediately after the cylinder top surface crosses the horizontal reference plane. This means that the drainage starts with stage 2 and is prolonged throughout stage 3. When the cylinder emerges out of the water, the liquid entrained by the front and by the rear of the cylinder forms a cascade (see Fig. 2, $y_c > 1$). This cascade continues until all the liquid has drained out.

IV. EXPERIMENTAL CONDITIONS AND LIMITATIONS

We aimed to approach as closely as possible a two-dimensional flow around the cylinder to allow comparison with 2D models. The two strategies followed to achieve this, i.e., cylinders with large aspect ratios and end plates, are here assessed by analyzing the film thickness as the cylinder emerges out of the bath and the flow lines obtained by PIV measurements.

Additionally, the impact of the starting depth d is evaluated, accounting for the acceleration (deceleration) length needed to reach constant velocity, but also for the limited size of the tank and the possible presence of end plates. In particular, the wake behind the cylinder during the immersed phase is characterized through PIV visualization.

A. 2D conditions: Aspect ratio

An interesting observable is the height $h^*/a = h(y_c = -1)/a$ reached by the fluid interface when the cylinder reaches the interface. For the water case, the measurement of h^*/a is presented in Fig. 3(a) as a function of the Froude number for six cylinders without end plates whose aspect ratio spreads between 1 and 12. Some typical videos (for five different aspect ratios and two pushing speeds) are presented in the Supplemental Material [39]. The figure also includes the case of the cylinder with the largest AR equipped with end plates. The height h^*/a, and thus the amount of entrained fluid, increases with the speed of the cylinder, i.e., with the Froude number, and with the aspect ratio. The observed behavior of the entrainment is in line with the observation of Haohao *et al.* [36], who reported that the waterfall breaking becomes more intense with increasing Froude number. The data were fitted using the empirical logarithmic law $h^*/a = A \ln(\text{Fr}) + B$ where A and B are fitting parameters [41]. These fitting parameters depend on AR with A between 0.07 and 17 and B between 0.32 and 0.60. The fits are shown as solid curves in Figs. 3(a) and 3(b).

The cylinders with AR $\leqslant$ 10 have a radius of 25 mm. For this family of cylinders, we observe that the curves $h^*/a(\text{Fr})$ become closer and closer with increasing AR. This is further illustrated in Fig. 3(c), which reports the values of h^*/a for Fr = 4 as a function of the aspect ratio. The red symbols (corresponding to the cylinders with a radius $a = 25$ mm) seem to saturate for large aspect ratios. One could thus expect that for even larger aspect ratios the curve $h^*/a(\text{Fr})$ would collapse. For comparison, the thickness h^*/a as a function of the Froude number is also shown for the AR = 12 cylinder, with and without end plates, but with a radius of 12.5 mm [magenta and cyan data points in Fig. 3(a)]. Surprisingly, the two curves significantly depart from that for AR = 10, even though a plateau was nearly reached in this latter case. On the other hand, the thickness $h^*/a(\text{Fr})$ is closer for the two AR = 12 cylinders with or without end plate. The values of $h^*/a(\text{Fr} = 4)$ for AR = 12, with and without end plates, are also reported in Fig. 3(c) (hollow and solid blue squares, respectively). The values are about 1.2 times larger than for the cylinder with AR = 10 and $a = 25$ mm.

These results seem to indicate that, in our experimental setup, the radius of the cylinder does play a role despite the normalization of h^*. A possible explanation might be the limited size of the tank, as the ratio between the cylinder radius and the tank lateral length or, more exactly, the ratio between the section surface of the cylinder and the surface of the bath changes. This lateral confinement seems responsible for the absolute value of the liquid elevation. Additionally, the comparison between the AR = 12 cylinder with and without end plates illustrates the role of end plates, even at a large aspect ratio: the fluid cannot escape around the cylinder end surfaces, thereby increasing the amount of liquid above the cylinder, i.e., the thickness h^*/a.

These results suggest that a large aspect ratio and end plates are necessary to approach two-dimensional conditions. We thus now compare for the oil case the AR = 12 ($a = 12.5$ mm) and the AR = 10 ($a = 25$ mm) cylinders both equipped with end plates in Fig. 3(b). The thickness h^*/a as a function of the Froude numbers shows the same qualitative behavior as for the water. We again observe that the results depend on the cylinder radius because of the confinement effect.
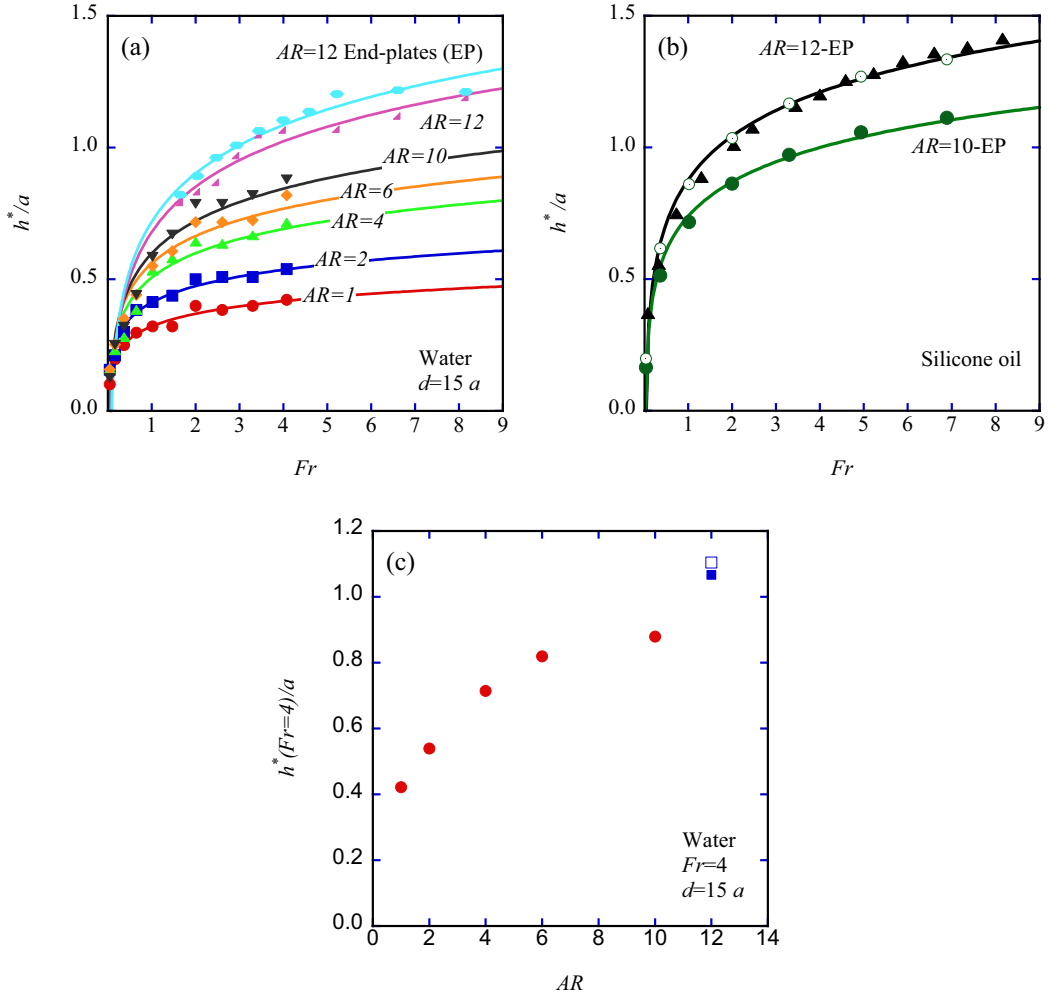
FIG. 3. (a) Water: Normalized thickness $h^*/a = h(y_c = -1)/a$ as a function of the Froude number for an initial depth $d = 15a$ and different aspects ratios AR. All cylinders are without end plates except for the largest $AR = 12$ (cyan). The different symbols represent the average value of seven experiments and the lines are logarithm fits (see text). (b) Silicone oil: Same plot as (a) but for two aspect ratios: green bullets $AR = 10$ ($d = 15a$) and black triangles $AR = 12$ ($d = 32a$), both cylinders equipped with end plates. The open circles correspond to the results obtained for $AR = 10$ multiplied by 1.2. (c) Water: Normalized thickness h^*/a for Fr $= 4$ extracted from (a) as a function of the aspect ratio. The red bullets correspond to cylinders with radius $a = 25$ mm without end plates, the solid blue square corresponds to the cylinder with $a = 12.5$ mm without end plates, and the hollow blue square corresponds to the latter cylinder but equipped with end plates.

Interestingly, we also find that, by simply multiplying the results obtained for AR $= 10$ by the same factor of 1.2 as previously, we obtain the same thickness as for AR $= 12$ [open circles in Fig. 3(b)]. Overall, we essentially observe that the largest aspect ratio is ideal and that the end plates do play a role. Moreover, the absolute value of h^*/a changes by a multiplicative factor when the radius of the cylinder is changed. This correction for the finite size of the tank is however difficult to predict *a priori*. In our case, we found a factor of 1.2 on h^*/a when doubling the radius.
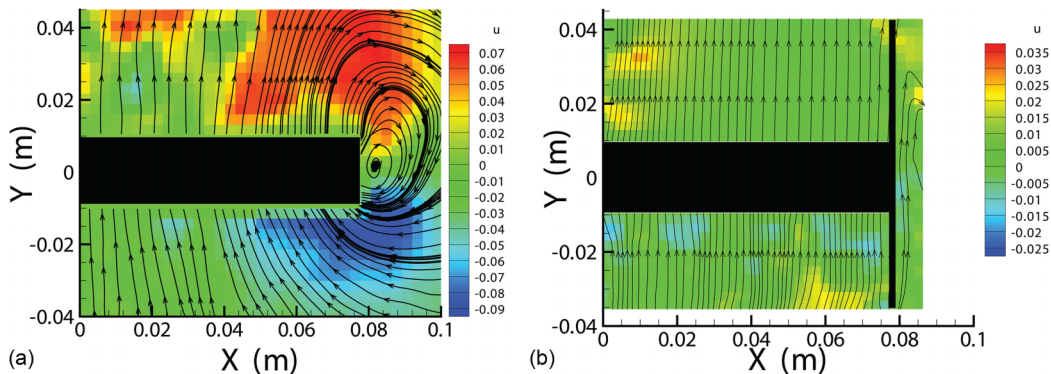
FIG. 4. Water: Side view of the flow field (*xy* plane) at $U = 0.5$ m/s (Fr = 2) for the AR = 12 ($a =$ 12.5 mm) cylinder (a) without and (b) with end plates. Streamlines in the absolute frame of reference and contour of the *x*-direction velocity. The images show a little bit more than half of the cylinder that is 150 mm long.

B. 2D conditions: End Plates

PIV measurements were performed during the cylinder motion below the free surface to determine whether the flow around the cylinder equipped with end plates is indeed two dimensional. The most favorable aspect ratio was investigated, namely AR = 12. The velocity field obtained by PIV is presented in Fig. 4(a) for the cylinder without end plates and in Fig. 4(b) with end plates. Without end plates, while the flow in the middle of the cylinder is mostly parallel and straight, it starts to exhibit a nonzero horizontal component when approaching the cylinder extremities. The flow is thus not fully two dimensional, except close to the center of the cylinder. With end plates, the streamlines are parallel along the whole length of the cylinder, as shown in Fig. 4(b). The water located above the cylinder cannot escape by the lateral side and two-dimensional conditions are well approximated.

Consequently, all results reported in the following are based on experiments with cylinders equipped with end plates, except in Sec. VI for the force measurements to avoid a significant bias of the measurements due to the weight of the end plates and the liquid entrainment by friction on their large surface.

C. Starting depth

For the comparison between the motion in the water and in oil, the cylinder with aspect ratio AR = 12 ($a = 12.5$ mm) and end plates was released from a depth $d = 24a$. Figure 5 shows the velocity vectors and vorticity contours from PIV measurements for two typical speeds corresponding to Froude numbers Fr = 0.33 (top) and 8.15 (bottom). The Reynolds numbers for the water case (left) are Re = 5000 and 25 000, while for the oil case (right) Re = 100 and 500, respectively. In the case of water, vortex shedding occurs even at a small speed (Fr = 0.33), breaking the symmetry of the flow. In particular, a pair of clockwise and anticlockwise vortices is located close to the cylinder and some weaker vortices previously shed in the wake are visible. As expected, the strength of these vortices increases with the cylinder velocity, and thus with the Froude and Reynolds numbers. The symmetry breaking influences both the entrainment and the collapse of the liquid behind the emerging cylinder. The situation is quite different in the case of the much more viscous silicone oil: there is no vortex shedding with a release depth of 24a and the wake remains symmetrical even for the most unfavorable sets of parameters considered here, i.e., highest speed and deepest possible starting depth (see Fig. 5(d)). The volume of liquid that is perturbed by the passage of the cylinder is thus rather well defined compared to the case of water. Note that the symmetry of the wake is
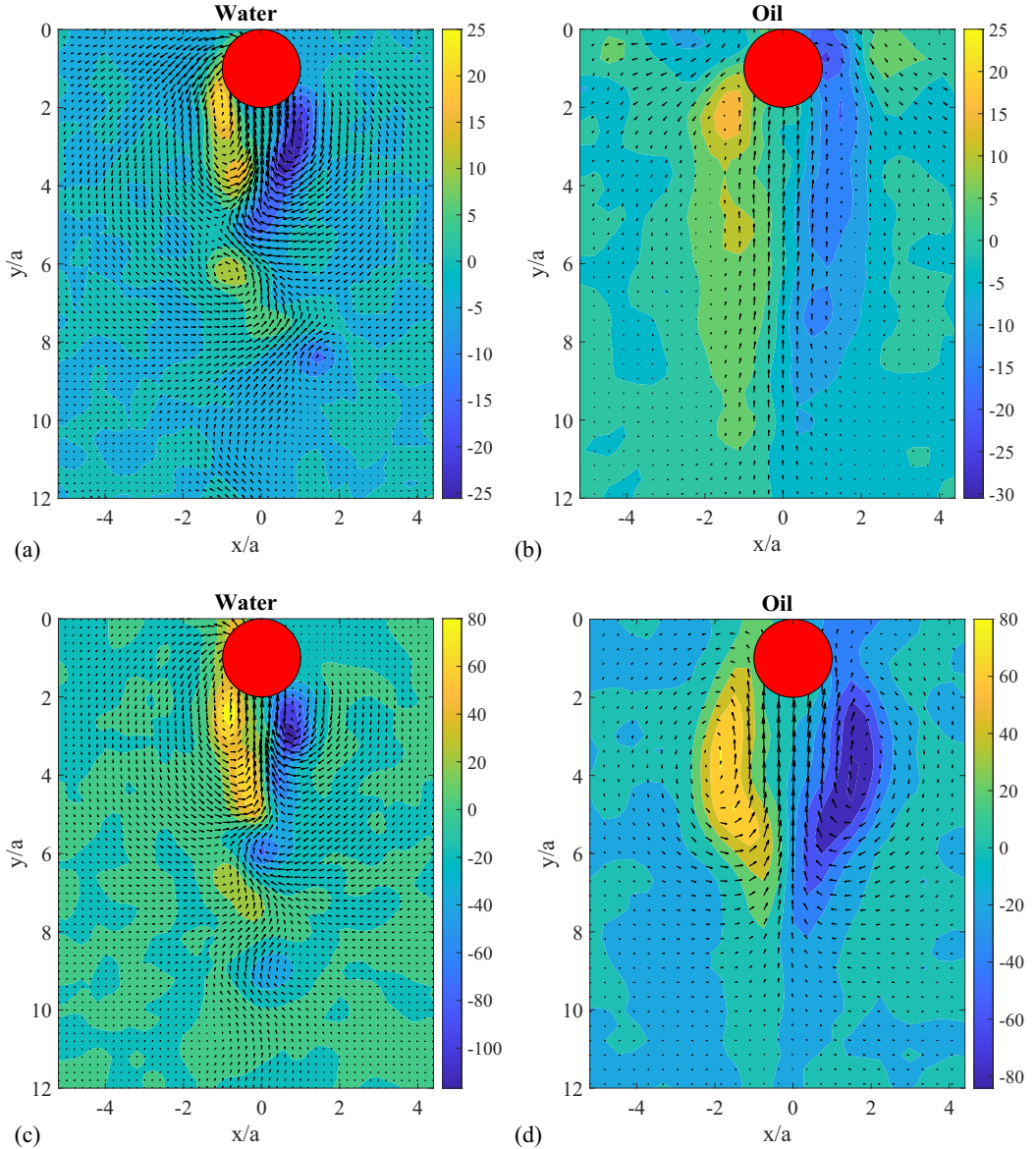
FIG. 5. Velocity vectors and vorticity contours in the xy plane through the cylinder midpoint from PIV measurements for the AR = 12 cylinder with end plates and a release depth $d = 24a$ in water (left: a, c) and oil (right: b, d) at Fr = 0.33 (top: a, b) and Fr = 8.5 (bottom: c, d).

important for any theoretical development. Furthermore, it has been shown that the evolution of the entrained liquid ahead of the cylinder is related to the dynamics of the wake [41].

Overall, the starting depth d does not influence the results concerning the deformation of the interface as soon as the depth is larger than a given value (three times the diameter of the cylinder according to Liju *et al.* [23]). From a practical point of view, we considered the release depth of at least $d > 12a$. This condition is stronger than the theoretical condition but we have to account here for the acceleration phase of the cylinder. Therefore, the cylinder's initial depth was set as deep as possible for each presented case. At last, it is important to mention that the maximum release depth

was constrained by the limited size of the tank and by the presence of the end plates. For an even larger d, one could possibly expect a destabilization of the wake and a subsequent vortex shedding to also occur for the oil case at the lower Reynolds number.

V. MOTION OF THE INTERFACE

The evolution of the thickness h between the top of the cylinder and the air-fluid interface was measured as a function of the normalized position y_c of the cylinder for different speeds (pushing mode) between 0.1 and 1.0 m/s. The motion of the interface was obtained by following the highest position reached by the interface while the cylinder was moving. The optical axis of the camera was horizontal and contained in the non-deformed interface plane. In so doing, the interface appeared in the middle of the image. Moreover, the camera was turned by $90°$ to have a maximum of pixels along the vertical direction since the sensor had a 10:9 ratio.

Before the experiments, the cylinder was placed just under the interface, and its position was recorded to determine the coordinate $y_c = -1$ on the image. Then, two pictures of the cylinder were taken below and above the interface to obtain the calibration pixels to millimeters (which differs due to difference in water and oil refraction index). The images were recorded close to the mid-plane of the cylinder to reach 2D conditions, even in the presence of end plates.

The contrast between the interface and the cylinder was sufficient to obtain the position of the interface and the cylinder by subtracting an image of the background, i.e., in the absence of the cylinder. The image resulting from the subtraction was then thresholded. Note that the position of the cylinder was obtained by tracking the lower position of the cylinder (the apex could not be tracked as easily as the bottom because of the interface deformation when the cylinder approached the interface). As a consequence, the position of the cylinder could only be measured when the bottom part of the cylinder was located in the bath. The position y_c of the cylinder was then extrapolated based on the position of the cylinder before $y_c = 0$. The linearity of y_c with time was also checked and the slope allowed us to confirm that the set-point speed was correct within a few percent.

In the case of silicone oil, measurements of $h(t)$ could be acquired over a long period of time thanks to the CCPS. In particular, because the oil wetted the cylinder, the entrained liquid slowly drained until reaching a thickness lower than 10 μm. Synchronizing the data obtained by the CCPS with $h(t)$ obtained by image analysis during the interface crossing, we could obtain the history of the film thinning over several time decades. The synchronization was achieved by triggering the data logger with the same signal as the high-speed camera. The recorded images allowed us to determine the time at which the cylinder crossed the interface.

A. Bulging stage ($y_c < -1$)

Figure 6 shows the thickness $h(y_c)$ for the water and the oil (AR $= 12$ equipped with end plates) for several speeds between 0.1 and 1.0 m/s as indicated by the Froude number. The starting depth was $d = 24a$ in water and $32a$ in silicone oil. In both cases, the same behavior is observed. The fluid thickness above the cylinder decreases monotonically as the cylinder approaches the air-fluid interface at $y_c = 0$. The decrease becomes more rapid when the cylinder approaches and crosses the interface. Because of liquid entrainment, the interface crossing becomes smoother with increasing the Froude number. The curves tend also to be closer and closer to each other. This convergence towards a limiting curve is to be correlated with the dependence of h^*/a on the Froude number Fr (see Fig. 3). These results suggest that the decrease of the thickness follows an exponential decay as a function of the position [i.e., as a function of time since $y_c(t) = Ut/a$].

The exponential behavior can be rationalized through a simple model which is similar to some extent to Ref. [42]. When the cylinder starts crossing the interface, the liquid layer surrounding the cylinder has a thickness h that depends on time and the position around the cylinder. This position can be parametrized by taking a cross section of the cylinder. Then, the thickness of oil around the circular section depends on the polar coordinate θ— i.e., the angle formed by the apex of the
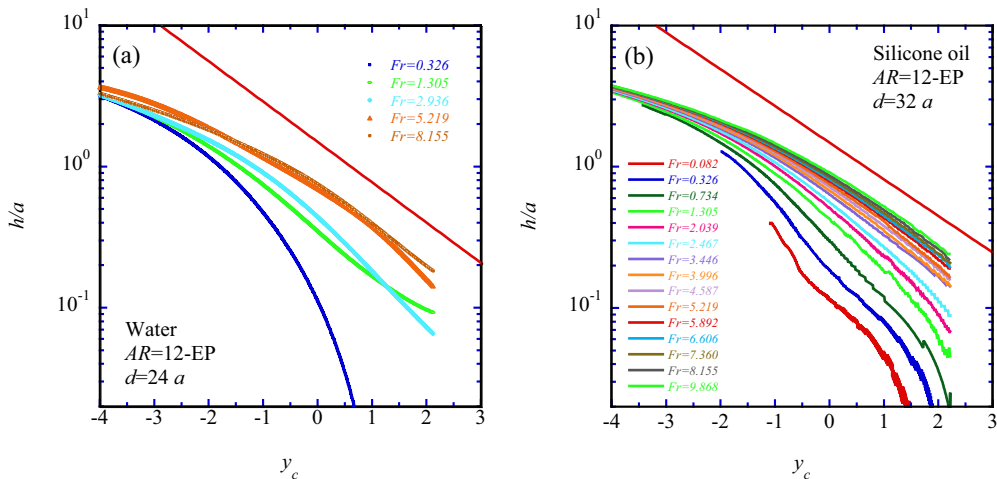
FIG. 6. Normalized thickness h/a of the liquid above the cylinder as a function of the cylinder position y_c for different Froude numbers: cylinder with AR = 12 and end plates in (a) water for $d = 24a$ and (b) silicone oil for $d = 32a$. The red lines represent an exponential decay function with a characteristic time $\tau = 19$ ms; to convert the time into y_c units, the exponential functions were calculated for the higher Fr in both cases, which corresponds to $U = 1.0$ m/s and 1.1 m/s for water and oil, respectively.

cross section, the center of the circle, and the considered element of fluid along the circle—. In the following, we consider the averaged value of the film thickness $\langle h(t, \theta) \rangle = h_m(t)$ along the perimeter of the cross section. Regarding the speed of the flow, because of the symmetry, the azimuthal velocity v_θ of the fluid vanishes at the cylinder apex ($\theta = 0$) and increases with θ; the maximum speed v_m is thus expected at $\theta = \pi/2$ (at least for $y_c \geqslant 0$). The volume V of liquid around the top half of the cylinder is given by $V \approx \pi a L \langle h_m \rangle$ and the flow rate $\dot{V} = 2L h_m v_m$. If the viscosity is neglected, the liquid is accelerated downwards by gravity and only the geometry of the flow is to be taken into account. We then find that $\dot{h}_m \propto h_m$ at first approximation. That means that the average thickness $h_m(t)$ experiences an exponential decay with time. The decay of h_m as a function of time was fitted by a decreasing exponential $\exp(-t/\tau)$. The red lines drawn in Fig. 6 correspond to the function $A_0 \exp[-y_c a/(U\tau)]$ where A_0 is an arbitrary constant and τ is the characteristic time. The characteristic time was found to be 19 ms (in both water and oil cases) and the reference speeds used to draw the lines were chosen as the highest speeds represented in Fig. 6, namely $U = 1.0$ and 1.1 m/s for water and oil, respectively. Finally, the characteristic time can be related to the "escape" speed of the fluid from the top of the cylinder. To a first approximation, we may compute the time τ_{fall} needed to fall from a height equal to the cylinder diameter: $\tau_{\text{fall}} \approx \sqrt{2a/g} \simeq 50$ ms. Note that this approximation overestimates the typical characteristic time since the liquid can escape by both sides of the cylinder.

B. Drainage stage ($y_c > -1$)

When the cylinder emerges out of the liquid, the entrained liquid drains. This process depends on the wetting properties of the liquid on the cylinder material. The water was found to dewet very quickly and the water film broke as soon as the cylinder was above the surface. On the other hand, in the case of oil, the liquid flew down from the top to the bottom of the cylinder forming a cascade back to the tank. The drainage time was much longer than with the water because (i) the oil wets the aluminum and (ii) the viscosity of the oil is 50 times higher than that of the water. Therefore, it was possible to directly measure the oil film thickness using the chromic confocal point sensor (CCPS). For this purpose, the cylinder was stopped at a precise position such that the top of the cylinder was
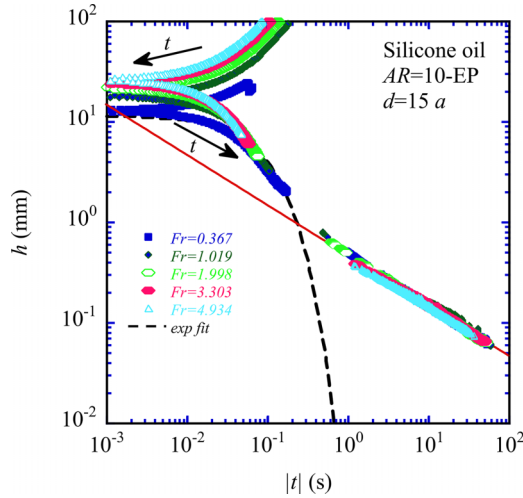
FIG. 7. Silicone oil: Thickness h as a function of the absolute value of the time for different Froude numbers (AR $= 10$ with end plates, $d = 15a$). The data above $h = 1$ mm were obtained using image analysis while the data below $h = 1$ mm were obtained using the CCPS. The arrows suggest the time direction. The continuous red line is a fit $t^{-1/2}$ of the data obtained with the CCPS; the dashed black line is the fit of the data corresponding to Fr $= 0.367$ for $t > 0$ by an exponential decay (see text).

located in the measurement range of the CCPS (this range is as large as 1.3 mm). Then, the CCPS measured the film thickness as a function of time (acquisition frequency of 2500 Hz). Knowing the deceleration rate, the maximum speed reached by the cylinder, and the time at which the cylinder crosses the interface, we synchronized the data obtained by image analysis and the direct thickness measurements.

Unlike the previous sections, data are here given for a cylinder with aspect ratio AR $= 10$ ($a = 25$ mm), instead of AR $= 12$ ($a = 12.5$ mm), equipped with end plates. The reason is that measurements using the CCPS are much more precise when the radius of curvature of the cylinder is larger. Although the pulling system allows precise vertical positioning of the cylinder, vibrations and oscillations of the system induce small lateral displacements that cause errors in the film thickness measurement. These errors can be reduced with a larger radius of curvature.

In Fig. 7, the thickness h from both sets of data (image analysis and CCPS) is presented as a function of time for different Froude numbers. The range of thickness measurements and the range of times considered are large. Because $t < 0$ s for $y_c < 0$, the absolute value of time is presented in logarithmic scale so that $h(|t|)$ is represented by cusp curves; the upper part corresponds to $h(t)$ when $t < 0$ s and the part below the cusp corresponds to $t > 0$ s. The data for times larger than 1 s were obtained through the CCPS. The superposition of the data from the image analysis and the CCPS provides the variation of the liquid thickness over five decades in time and nearly four decades in thickness. The data from the CCPS are found to be the natural prolongation of the data obtained by image analysis. Moreover, the drainage curves overlap for $t > 1$ s, indicating that the drainage dynamics does not depend much on the initial condition, i.e., the cylinder velocity U here. This confirms the fact that the initial thickness of the draining film above an object is not relevant. The red line in Fig. 7 is a fit of the CCPS data using a power law of the time, $h \propto t^{-1/2}$, while the black dashed line is an exponential decay fit of h at the first instant after the interface crossing. This scaling was also obtained for a static cylinder on which a constant flow of liquid is poured [42]. The exponential decay (when $t > 0$ s) is determined by a characteristic time $\tau = 93$ ms (in the case of the cylinder AR $= 10$, $\tau_{\text{fall}} \simeq 71$ ms). The regime change occurs at approximately $t \simeq 250$ ms and $h \simeq 1$ mm (see Fig. 7) and reflects the fact that the fluid viscosity becomes dominant when the
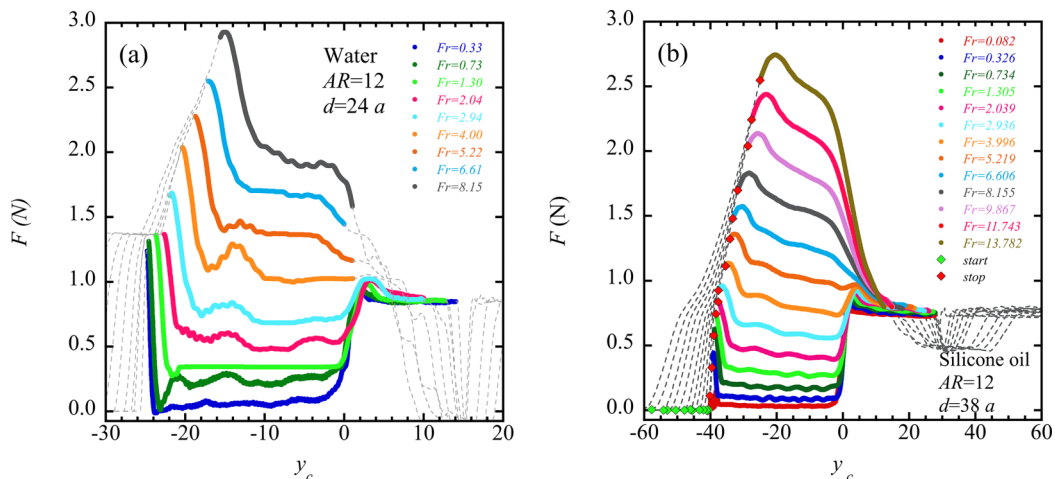
FIG. 8. Force applied to the $AR = 12$ cylinder without end plates during its motion as a function of its position y_c for different Froude numbers (a) in water from $d = 24a$ and (b) in silicone oil from $d = 38a$. In (b) the acceleration and deceleration phases are shown as dashed gray lines and do not correspond to the actual y_c since during the acceleration $y_c \neq Ut/a$. Additionally, the beginning and the end of the acceleration are indicated by the green and red diamonds, respectively.

film thins. Remarkably, irrespective of the crossing speed, the change of behavior occurs almost at the same time and for the same critical thickness. The change of regime between the exponential decay and the power law occurs at time $t \approx 0.2$ s for a thickness $h \approx 1$ mm. For small thicknesses, a lubrication equation applies (see, e.g., Ref. [42]). The lubrication condition reads

$$\mathrm{Re}_f \frac{h}{\ell} \ll 1,$$

with $\ell \approx \pi a$ and the Reynolds number of the flow $\mathrm{Re}_f = Vh/\nu$ where ν is the cinematic viscosity and $V \approx \sqrt{2ga}$. In so doing, we obtain that the change of regime should occur when

$$h \ll \sqrt{\pi \nu / 2} \left(\frac{a}{2g} \right)^{1/4}$$

which provides a crossing over for a thickness lower than a critical value $h_c \approx 1.7$ mm. This value is compatible with the crossing over found experimentally (see Fig. 7).

VI. FORCE MEASUREMENTS

The force measurements allow a global measurement from the start to the complete interface crossing. When the cylinder is below the surface, the force results from the contributions of the cylinder weight, the buoyancy, and the drag. When the cylinder is out of the liquid, the buoyancy and drag vanish but the weight of the entrained liquid adds to the cylinder weight. Moreover, inertial contributions are also present during the acceleration and deceleration phases.

The evolution of the force in water and oil is reported as a function of the cylinder position for different Froude numbers (pulling speeds) in Fig. 8. The aspect ratio used for these measurements was restricted to the highest considered value of 12 since the 2D conditions are more closely satisfied when the cylinder is long. Note that the end plates cannot be used during the force measurement experiments because they can entrain large quantities of oil (dip-coated film along a vertical plane) and, in the case of water, generate waves at the surface of the water when crossing the interface.
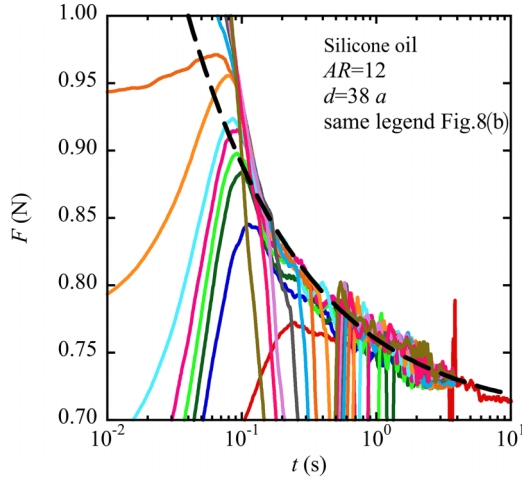
FIG. 9. Force applied to the cylinder as a function of time [same conditions as Fig. 8(b) for $t > 0$ s using a semilogarithmic scale]. The dashed curve represents a $t^{-1/2}$ trend.

Experimentally, the signal from the data logger provides the curve $F(t)$ (see Fig. 9). The reference force $F = 0$ N corresponds to the measured force when the cylinder is at rest and under the liquid surface. To compare the force measurements for the different speeds considered, the time series are converted into the position of the cylinder: a simple transformation following the rectilinear motion was applied, namely $y_c = Ut/a$, with $t = 0$ s when the cylinder is located at $y_c = 0$. This means that, during the acceleration and deceleration phases, the conversion $t \rightarrow y_c$ following the linear law does not hold. We choose nonetheless to present the curves including this bias to show the force variation during the complete motion of the cylinder. In Fig. 8, the data points corresponding to the acceleration and deceleration phases have been suppressed in the case of water. In the case of oil, the acceleration phase is delimited by a green diamond when the acceleration stage starts and a red diamond when it ends. Both acceleration and deceleration phases are indicated by gray dashed lines.

Figure 8 clearly shows that, until the later drainage phase, the force level strongly increases with the cylinder speed (Froude number), as expected. We can also identify different stages in the evolution of the force. The force first strongly increases during the acceleration phase (dashed line at low values of y_c for the oil) and reaches a maximum shortly after the end of the acceleration. Then, the force starts dropping before reaching a plateau (or a region of lower decreasing rate at high Fr for the oil case). This plateau is particularly marked at low Froude numbers (Fr $\lesssim 4$) and extends until shortly before the cylinder reaches the interface ($y_c < -1$). This plateau region is representative of the drag force acting on the cylinder in the liquid bath. In particular, the magnitude F_d of the force was evaluated when the plateau was visible and was found to be proportional to the Froude number. This corresponds to a dependence on the square of the motion velocity, U^2, consistent with hydrodynamic drag. Approaching $y_c = -1$, the evolution of the force shows significant qualitative differences depending on the Froude number (see also Vincent *et al.* [41]). This behavior is observed for both water and oil. In particular, below Fr ≈ 4 the force abruptly increases shortly before and during interface crossing, reaching a maximum after the cylinder has exited the bath. This force increase reflects the fact that the reduction of the buoyancy contribution dominates the reduction of the drag when the cylinder exits the bath. For Froude numbers larger than Fr ≈ 4, the situation is inverted: the decrease of the drag force is larger than that of the buoyancy so that the overall force decreases during the interface crossing. At Fr ≈ 4 (or Fr ≈ 5 for the oil), the combined contribution of buoyancy and drag for the cylinder in the liquid bath is more or less equal to the weight of the entrained liquid when the cylinder is out of the bath.

Once the cylinder has emerged out of the bath, the measured force corresponds to the weight of the cylinder (minus the buoyancy) plus the weight of the entrained liquid. Consequently, following the increase at low Fr and decrease at large Fr, the force converges to similar values for all Froude numbers but remains nonetheless larger for higher Froude numbers owing the the larger amount of liquid entrained at larger speeds. During drainage, the force then slowly and monotonously decreases towards the equilibrium value, i.e., the weight of the cylinder minus the buoyancy force (this follows from the definition of the reference force $F = 0$ N). The bump observed for Fr $\lesssim 4$ just after interface crossing corresponds thus to the weight of the entrained liquid. Lastly, note that the temporary force decrease at large y_c [dashed lines in Fig. 8(b)] is due to inertial effects during the deceleration of the cylinder.

Finally, the force in oil is reported as a function of time in Fig. 9 when the cylinder is out of the liquid bath, namely during the drainage phase, $t > 0$ s. The force measurements $F(t)$ for all Froude numbers seem to converge towards a common curve. The dashed curve represents a power law, i.e., $F \propto t^{-1/2}$. This power law is compatible with the observed law of thickness decay found in Fig. 7 and with the common decay law found in the literature (e.g., Ref. [19]).

VII. CONCLUSION

In this paper, an experimental setup has been developed to study the forced exit dynamics of a fully submerged horizontal cylinder. Two cases were considered: the water and the silicone oil (50 cS) for Froude numbers lower than 15.

The aspect ratio of the cylinder was taken as large as possible and equipped with end plates to observe as close as possible two-dimensional flow conditions at the center of the cylinder. The best combination was checked by analyzing the flow in the liquid bath through PIV measurements and by evaluating the dependence of the interface displacement on the aspect ratio.

The wake of the cylinder was studied during the displacement of the cylinder in the bath. PIV measurements showed the formation of clockwise and anticlockwise vortices during the cylinder's upward motion. The vortices shed in the wake were quickly diffused and large vortices were only observed in the vicinity of the cylinder. These vortices remained symmetrically positioned in the case of the silicone oil (lower Reynolds number), and this even for long-traveling cases ($d > 20a$). In the case of water, the vortices were detached and asymmetrical.

The thickness of the fluid layer above the cylinder was also measured through two different techniques: image analysis when the thickness was above 1 mm and chromatic confocal point sensor for smaller thicknesses during the drainage phase. The combination and the synchronization of both data allowed evidence of a change of regime in the thinning of the entrained liquid at the apex of the cylinder. Just after the interface crossing, the thickness of the liquid decreased according to an exponential decay in time. For times larger than $\simeq 250$ ms and thicknesses lower than $\simeq 1$ mm, the thinning followed a power scaling law of the form $t^{-1/2}$.

Finally, the force measurements carried out during the upward motion of the AR $= 12$ cylinder allowed the estimation of the net drag force. As expected, results showed that the net drag and entrained forces increased with the cylinder's upward velocity. Consequently, a particular Froude number exists above which the force drops after the crossing of the interface. The force measurements also confirmed that the drainage dynamics evolved according to the square root of time.

In the future, the overall deformation of the interface due to more complex shaped objects should be studied. Indeed, when the object approaches the interface, the interface first deforms according to a bump before revealing the shape of the object during the drainage stage. The force variations could also indicate the influence of the wake on the liquid entrainment. However, the speed of the crossing has been confirmed to have a minimal impact on the drainage dynamics of the fluid around the object.

---

[1] B. Chang, J. Myeong, E. Virot, C. Clanet, H.-Y. Kim, and S. Jung, Jumping dynamics of aquatic animals, J. R. Soc. Interface **16**, 20190014 (2019).

[2] B. Chang, M. Croson, L. Straker, and S. Jung, How seabirds plunge-dive without injuries, Proc. Natl. Acad. Sci. USA **113**, 12006 (2016).

[3] R. Challa, S. C. Yim, V. Idichandy, and C. Vendhan, Rigid-object water-entry impact dynamics: Finite-element/smoothed particle hydrodynamics modeling and experimental validation, J. Offshore Mech. Arct. Eng. **136**, 031102 (2014).

[4] R. Challa, V. G. Idichandy, C. P. Vendhan, and S. Yim, An experimental study on rigid-object water-entry impact and contact dynamics, in *Proceedings of the ASME 2010 29th International Conference on Ocean, Offshore and Arctic Engineering* (ASME, Shanghai, 2010), Vol. 4, pp. 383–391.

[5] A. Motta, R. Challa, S. C. Yim, and C. Q. Judge, Numerical modeling of hydrodynamic impact and local slamming effects, in *SNAME 13th International Conference on Fast Sea Transportation* (Estados Unidos, Washington DC, 2015).

[6] Q. Yang and W. Qiu, Numerical simulation of water impact for 2D and 3D bodies, Ocean Eng. **43**, 82 (2012).

[7] V. V. Nair and S. Bhattacharyya, Water entry and exit of axisymmetric bodies by CFD approach, J. Ocean. Eng. Sci. **3**, 156 (2018).

[8] B. Zhou, Z. Zhao, Q. Dai, W. Yao, X. Liu, Y. Zhang, A. Wang, and H. Zhang, Numerical study on the cavity dynamics of water entry and exit for a high-speed projectile crossing a wave, Phys. Fluids **36**, 063321 (2024).

[9] L. Landau and V. Levich, Dragging of a liquid by a moving plate, in *Dynamics of Curved Fronts*, edited by P. Pelcé (Academic Press, Marseille, 1988).

[10] L. Landau and V. Levich, Dragging of a liquid by a moving plate, Acta Physicochim. URSS **17**, 42 (1942).

[11] A. de Ryck and D. Quéré, Fluid coating from a polymer solution, Langmuir **14**, 1911 (1998).

[12] J. Seiwert, C. Clanet, and D. Quéré, Coating of a textured solid, J. Fluid Mech. **669**, 55 (2011).

[13] H. Dixit and G. Homsy, The elastocapillary landau-levich problem, J. Fluid Mech. **735**, 1 (2013).

[14] E. Benilov, S. Chapman, J. McLeod, J. Ocknedon, and Z. V.S., On liquid films on an inclined, J. Fluid Mech. **663**, 53 (2010).

[15] S. Weinstein and K. Ruschak, Dip coating on a planar non-vertical substrate in the limit of negligible surface tension, Chem. Eng. Sci. **56**, 4957 (2001).

[16] E. Jambon-Puillet, P. G. Ledda, F. Gallaire, and P. T. Brun, Drops on the underside of a slightly inclined wet substrate move too fast to grow, Phys. Rev. Lett. **127**, 044503 (2021).

[17] S. Eghbali, S. Djambov, and F. Gallaire, Stability of a liquid layer draining around a horizontal cylinder: Interplay of capillary and gravity forces, Phys. Rev. Fluids **9**, 063903 (2024).

[18] O. Reynolds, On the theory of lubrication and its application to mr. beauchamp tower's experiments, including an experimental determination of the viscosity of olive oil, Philos. Trans. R. Soc. **177**, 157 (1886).

[19] D. Chan and R. Horn, The drainage of thin liquid films tween solid surfaces, J. Chem. Phys. **83**, 5311 (1985).

[20] J. Coons, P. Halley, S. McGlashan, and T. Tran-Cong, A review of drainage and spontaneous rupture in free standing thin films with tangentially immobile interfaces, Adv. Colloid Interface Sci. **105**, 3 (2003).

[21] M. Bhamla, C. Giacomin, C. Balemans, and G. Fuller, Influence of interfacial rheology on drainage from curved surfaces, Soft Matter **10**, 6917 (2014).

[22] Q. Wu, B. Ni, X. Bai, B. Cui, and S. Sun, Experimental study on large deformation of free surface during water exit of a sphere, Ocean Eng. **140**, 369 (2017).

[23] P.-Y. Liju, R. Machane, and A. Cartellier, Surge effect during the water exit of an axisymmetric body traveling normal to a plane interface: experiments and bem simulation, Exp. Fluids **31**, 241 (2001).

[24] S. Moshari, A. H. Nikseresht, and R. Mehryar, Numerical analysis of two and three dimensional buoyancy driven water-exit of a circular cylinder, Int. J. Nav. Archit. Ocean Eng. **6**, 219 (2014).

[25] T. T. Truscott, B. P. Epps, and R. H. Munns, Water exit dynamics of buoyant spheres, Phys. Rev. Fluids **1**, 074501 (2016).

[26] P. Bourrier, E. Guyon, and J. Jorre, The pop off effect: different regimes of a light ball in water, Eur. J. Phys. **5**, 225 (1984).

[27] K. Takamure and T. Uchiyama, Effect of Froude number on the motion of a spherical particle launched vertically upward in water, Exp. Therm Fluid Sci. **128**, 110453 (2021).

[28] I. Ashraf and S. Dorbolo, Effect of the surface dimples on the exit dynamics of a sphere at a constant velocity, Appl. Ocean Res. **147**, 103996 (2024).

[29] X.-s. Chu, K. Yan, Z. Wang, K. Zhang, G. Feng, and W.-q. Chen, Numerical simulation of water-exit of a cylinder with cavities, J. Hydrodyn **22**, 877 (2010).

[30] T. H. Havelock, The forces on a circular cylinder submerged in a uniform stream, Proc. R. Soc. Lond. A **157**, 526 (1936).

[31] M. Greenhow and W.-M. Lin, Nonlinear-free surface effects: experiments and theory, MIT Internal Report 83-19 (1983).

[32] M. Greenhow and S. Moyo, Water entry and exit of horizontal circular cylinders, Philos. Trans. R. Soc. London, Ser. A **355**, 551 (1997).

[33] J. G. Telste, Inviscid flow about a cylinder rising to a free surface, J. Fluid Mech. **182**, 149 (1987).

[34] B. Ni, A. Zhang, and G. Wu, Simulation of complete water exit of a fully-submerged body, J. Fluids Struct. **58**, 79 (2015).

[35] I. Ashraf and S. Dorbolo, Exit dynamics of a square cylinder, Ocean Eng. **297**, 117106 (2024).

[36] H. Haohao, S. Yanping, Y. Jianyang, C. Fu, and L. Tian, Numerical analysis of water exit for a sphere with constant velocity using the lattice boltzmann method, Appl. Ocean Res. **84**, 163 (2019).

[37] G. Miao, Hydrodynamic forces and dynamic responses of circular cylinders in wave zones, Ph.D. thesis, Dept. of Marine Hydrodynamics, NTH, Trondheim, 1989.

[38] X. Wei, D. Li, J. Lei, J. Li, J. Rivero-Rodriguez, F. Lin, D. Wang, and B. Scheid, Exit dynamics of a sphere launched underneath a liquid bath surface, Phys. Rev. Fluids **9**, 054003 (2024).

[39] See Supplemental Material at http://link.aps.org/supplemental/10.1103/PhysRevFluids.9.124005 for ten high speed movies with two different speeds and five different aspect ratios.

[40] W. Thielicke and E. Stamhuis, PIVLAB–towards user-friendly, affordable and accurate digital particle image velocimetry in matlab, J. Open Res. Softw. **2**, e30 (2014).

[41] L. Vincent, J. Rivero, R. Falla, I. Ashraf, V. E. Terrapon, S. Dorbolo, and B. Scheid, Inertial exit dynamics of a horizontal cylinder out of a liquid bath, J. Fluid Mech. (to be published).

[42] D. Takagi and H. E. Huppert, Flow and instability of thin films on a cylinder and sphere, J. Fluid Mech. **647**, 221 (2010).